Electric field modulated valley- and spin-dependent electron retroreflection and Klein tunneling in a tilted *n-p-n* junction of monolayer $1T'$-MoS_2

Dali Wang,[1,3,*] Anqi Hu,[1] Jian-Ping Lv,[1] and Guojun Jin[2,3,†]

[1]*Department of Physics and Anhui Key Laboratory of Optoelectric Materials Science and Technology, Anhui Normal University, Wuhu 241002, China*

[2]*School of Physics Science and Technology, Kunming University, Kunming 650214, China*

[3]*National Laboratory of Solid State Microstructures, Department of Physics, and Collaborative Innovation Center of Advanced Microstructures, Nanjing University, Nanjing 210093, China*

(Received 21 September 2022; accepted 21 December 2022; published 3 January 2023)

We study the electronic transport properties in a tilted *n-p-n* junction of monolayer $1T'$-MoS_2 under a vertical electric field. The analytical derivations and numerical results show that, since the spin degeneracy of the anisotropic bands of monolayer $1T'$-MoS_2 is lifted by the electric field E_z, electrically tunable valley- and spin-dependent electron retroreflection occurs in the tilted *n-p-n* junction. It is also found that when the electric field E_z is adjusted to a critical value E_c, valley- and spin-dependent Klein tunneling happens in the *n-p-n* junction, and the incident angle of Klein tunneling depends on the tilt angle of the junction. Especially, for a certain specific tilt angle, in the case of normal incidence, only a spin-up electron from the K valley can undergo Klein tunneling. Our work offers an efficient mechanism to modulate valley- and spin-dependent electron retroreflection and Klein tunneling in anisotropic tilted Dirac systems.

DOI: 10.1103/PhysRevB.107.035301

I. INTRODUCTION

Since the celebrated discovery of monolayer graphene, various other two-dimensional monolayer materials made from group III-VI elements have emerged one after another, such as silicene [1], germanene [2], stanene [3], phosphorene [4–6], arsenene [7,8], antimonene [9], and borophene [10–12]. Meanwhile, layered transition metal dichalcogenides (TMDCs), which have the general chemical formula MX_2 with $M = (\mathrm{W}, \mathrm{Mo})$ and $X = (\mathrm{Te}, \mathrm{Se}, \mathrm{S})$, have also been researched widely, both experimentally and theoretically [13–22]. Monolayer TMDCs possess a variety of polytypic structures including $1H$, $1T$, and $1T'$ [15,17]. Unlike its stable $1H$ counterpart, monolayer $1T'$-MX_2 is typically unstable and undergoes a spontaneous lattice distortion to form a period-doubling zigzag chain, which leads to the formation of $1T'$-MX_2 [15,17,23–28]. In this type of materials, $1T'$-MoS_2 is a typical representative of $1T'$-MX_2. It has been shown that monolayer $1T'$-MoS_2 possesses tilted Dirac bands with a spin-orbit coupling (SOC) gap (∼0.08 eV) at each Dirac point and a large band-inverted gap (∼0.6 eV) at the Γ point in the Brillouin zone. Furthermore, the anisotropic band structure of monolayer $1T'$-MoS_2 is tunable by a vertical electric field, leading to strong spin splitting of the doubly degenerate bands around the Dirac points [15].

In addition to $1T'$-MX_2, other anisotropic monolayer Dirac materials, such as 8-*Pmmn* borophene [29], α-SnS_2 [30], $TaCoTe_2$ [31], and $TaIrTe_4$ [32], also possess tilted Dirac bands in the vicinity of Dirac points. The band tilting in these anisotropic Dirac systems induces a strong anisotropy in physical properties, including anisotropic plasmons [33,34], optical conductivities [35,36], Weiss oscillation [37], Fabry-Pérot resonances [38], Ruderman-Kittel-Kasuya-Yosida (RKKY) interactions [39], and thermoelectric effects [40]. As is well known, the electrons in isotropic materials undergo specular reflection at an interface due to the fact that the group velocity component parallel to the interface is locked to the corresponding wave vector, while in anisotropic materials, the anisotropic band structure may release the locking relation, which makes electron retroreflection possible [41–43]. Recently, it was reported that electron retroreflection and Klein tunneling may be generated in 8-*Pmmn* borophene-based tunnel junctions by changing the direction of the junction [44–46]. But from practical applications, it is inconvenient to adjust the direction of the junction for a given device. Therefore, the purpose of this paper is to explore an electrically tunable electron retroreflection and Klein tunneling in a tilted *n-p-n* junction of monolayer $1T'$-MoS_2.

The rest of the paper is organized as follows. In Secs. II and III, the model and basic formalism are constructed and derived. In Secs. IV and V, the numerical results and theoretical analyses are presented and discussed. Finally, a brief summary is given in Sec. VI.

II. BAND STRUCTURE UNDER AN EXTERNAL FIELD

In the presence of a vertical electric field, the low-energy $\boldsymbol{k}\cdot\boldsymbol{p}$ Hamiltonian for monolayer $1T'$-MoS_2 is given by [15]

$$\mathcal{H} = \mathcal{H}_{\boldsymbol{k}\cdot\boldsymbol{p}} + \mathcal{H}_{E_z}, \tag{1}$$

*wangdali@ahnu.edu.cn
†gjin@nju.edu.cn

where

$$\mathcal{H}_{\boldsymbol{k}\cdot\boldsymbol{p}} = \begin{pmatrix} E_p(k_x,k_y) & 0 & -iv_1\hbar k_x & v_2\hbar k_y \\ 0 & E_p(k_x,k_y) & v_2\hbar k_y & -iv_1\hbar k_x \\ iv_1\hbar k_x & v_2\hbar k_y & E_d(k_x,k_y) & 0 \\ v_2\hbar k_y & iv_1\hbar k_x & 0 & E_d(k_x,k_y) \end{pmatrix}, \quad (2)$$

and

$$\mathcal{H}_{E_z} = \alpha E_z \begin{pmatrix} 0 & 0 & 1 & 0 \\ 0 & 0 & 0 & 1 \\ 1 & 0 & 0 & 0 \\ 0 & 1 & 0 & 0 \end{pmatrix}. \quad (3)$$

Here, $E_p = -\delta_p - \hbar^2 k_x^2/(2m_x^p) - \hbar^2 k_y^2/(2m_y^p)$ and $E_d = \delta_d - \hbar^2 k_x^2/(2m_x^d) - \hbar^2 k_y^2/(2m_y^d)$ are the on-site energies of p and d orbitals in monolayer $1T'$-MoS_2, respectively, with $-\delta_p$ and δ_d being the corresponding energies of p and d orbitals at the Γ point, and $m_x^{p(d)}$ and $m_y^{p(d)}$ being the effective masses of the p (d) band in the x and y directions. In addition, v_1 and v_2 denote the velocities along the x and y directions, α is the electrical coefficient, and E_z is a vertical electric field that can break inversion symmetry and introduce a strong Rashba splitting of the doubly degenerate bands around the Dirac points. The above parameters were obtained by fitting the first-principles band structures [15]. They are as follows: $\delta_p = 0.46$ eV, $\delta_d = 0.20$ eV, $v_1 = 3.87 \times 10^5$ m/s, $v_2 = 0.46 \times 10^5$ m/s, $m_x^p = 0.50m_0$, $m_y^p = 0.16m_0$, $m_x^d = 2.48m_0$, and $m_y^d = 0.37m_0$ with m_0 being the free electron mass.

For Eq. (1), we perform the unitary transformation [47]. Then, the spin texture is resolved and the Hamiltonian of the system is transformed to a block-diagonal form. In the vicinity of the two Dirac points located at $\Lambda = \pm(0, 1.46)$ nm^{-1} [15], we further make the Taylor expansions and finally obtain

$$\mathcal{H}'_\eta = \begin{pmatrix} \boldsymbol{h}_{\eta\uparrow}(\boldsymbol{k}) & \boldsymbol{0} \\ \boldsymbol{0} & \boldsymbol{h}_{\eta\downarrow}(\boldsymbol{k}) \end{pmatrix}, \quad (4)$$

where the top-left block,

$$\boldsymbol{h}_{\eta\uparrow}(\boldsymbol{k}) = \hbar k_x v_1 \tau_y - \hbar k'_y(\eta v_- \tau_0 + \eta v_+ \tau_z + v_2 \tau_x) + (\alpha E_z - \eta\Delta_{\rm so})\tau_x, \quad (5)$$

corresponds to the spin-up states, and the bottom-right block, $\boldsymbol{h}_{\eta\downarrow}(\boldsymbol{k}) = \boldsymbol{h}^*_{-\eta\uparrow}(-\boldsymbol{k})$, corresponds to the spin-down states. Here, τ_0 and τ_i ($i = x, y, z$) stand for the Pauli matrices in the band pseudospin space, $k'_y = k_y - \eta k_0$ is the wave vector relative to the Dirac points with $k_0 = 1.46$ nm^{-1}, $\eta = \pm 1$ stands for the valley index (K or K'), $\Delta_{\rm so} = v_2\hbar k_0$ ($\sim$0.04 eV) represents the SOC gap ($2\Delta_{\rm so}$) at the Dirac points, and $v_\pm = \hbar k_0(m_y^d \pm m_y^p)/(2m_y^p m_y^d)$. Since $\mathcal{H}'_\eta$ is block diagonal, the eigenstates can be written as

$$\psi_{\eta\uparrow} = \begin{pmatrix} \phi_{\eta\uparrow} \\ \boldsymbol{0} \end{pmatrix}, \quad \psi_{\eta\downarrow} = \begin{pmatrix} \boldsymbol{0} \\ \phi_{\eta\downarrow} \end{pmatrix}, \quad (6)$$

where $\boldsymbol{0}$ is a two-component zero vector, and $\phi_{\eta\uparrow}$ ($\phi_{\eta\downarrow}$) is the eigenvector of $\boldsymbol{h}_{\eta\uparrow}$ ($\boldsymbol{h}_{\eta\downarrow}$). It is noted that $\psi_{\eta\uparrow}$ is related to $\psi_{\eta\downarrow}$ by time-reversal symmetry, i.e.,

$$\psi_{\eta\downarrow}(\boldsymbol{k}) = -i\sigma_y \mathcal{K} \otimes \mathbb{I}_{2\times 2}\psi_{-\eta\uparrow}(-\boldsymbol{k}). \quad (7)$$

Here, $\mathbb{I}_{2\times 2}$ is a 2×2 identity matrix, $\mathcal{K}$ denotes the complex conjugation operator, and σ_y is the Pauli matrix in real-spin space.

From Eq. (4), it follows that the energy dispersion around the Dirac points reads

$$E^{\pm}_{\eta s} = -\eta\hbar v_- k'_y \pm \sqrt{(\hbar v_1 k_x)^2 + (\hbar v_+ k'_y)^2 + [\hbar v_2 k'_y + (\eta\Delta_{\rm so} - s\alpha E_z)]^2}, \quad (8)$$

where $\pm$ corresponds to the conduction and valence bands, and $s = \pm 1$ stands for electron spin up ($\uparrow$) and spin down ($\downarrow$), respectively. In the absence of a vertical electric field ($E_z = 0$), the energy bands of monolayer $1T'$-MoS_2 are spin degenerate, and SOC gaps ($2\Delta_{\rm so}$) exist at the Dirac points. For each valley, the shift of the conduction-band bottom and valence-band top of the tilted energy bands along the k_y direction is

$$\chi = \frac{2v_- v_+ \Delta_{\rm so}}{\hbar(v_2^2 + v_+^2)\sqrt{v_2^2 + v_+^2 - v_-^2}}, \quad (9)$$

and their corresponding energy difference is

$$\Delta = \frac{2v_+\sqrt{v_2^2 + v_+^2 - v_-^2}}{v_2^2 + v_+^2}\Delta_{\rm so} \approx 1.83\Delta_{\rm so}, \quad (10)$$

which is smaller than the SOC gap ($2\Delta_{\rm so}$) at the Dirac points, as can be seen in Fig. 1(a). However, in the presence of a vertical electric field, as shown in Figs. 1(b) and 1(c), the spin degeneracy of the energy bands of monolayer $1T'$-MoS_2 is lifted, and then for each valley, the shift of the subbands with the same spin along the k_y direction and the corresponding indirect energy gap become valley and spin dependent, which read

$$\chi_{\eta s} = \frac{2v_- v_+ |\eta s\Delta_{\rm so} - \alpha E_z|}{\hbar(v_2^2 + v_+^2)\sqrt{v_2^2 + v_+^2 - v_-^2}} \quad (11)$$

and

$$\Delta_{\eta s} = \frac{2v_+\sqrt{v_2^2 + v_+^2 - v_-^2}}{v_2^2 + v_+^2}|\eta s\Delta_{\rm so} - \alpha E_z|. \quad (12)$$

Hence, the vertical electric field E_z can effectively modulate the band structure of monolayer $1T'$-MoS_2. As the electric field E_z increases, the band gap first decreases to zero at a critical field $E_c = \Delta_{\rm so}/\alpha$ ($\sim$1.42 V nm^{-1}) [15] and then reopens, as shown in Figs. 1(b) and 1(c).

In order to further explore the band structure of monolayer $1T'$-MoS_2 under an electric field, in Fig. 2 we show the bottom of the valley-spin resolved subbands in the positive-energy region ($E^{+,\rm b}_{\eta s}$) and the top of the corresponding subbands in the

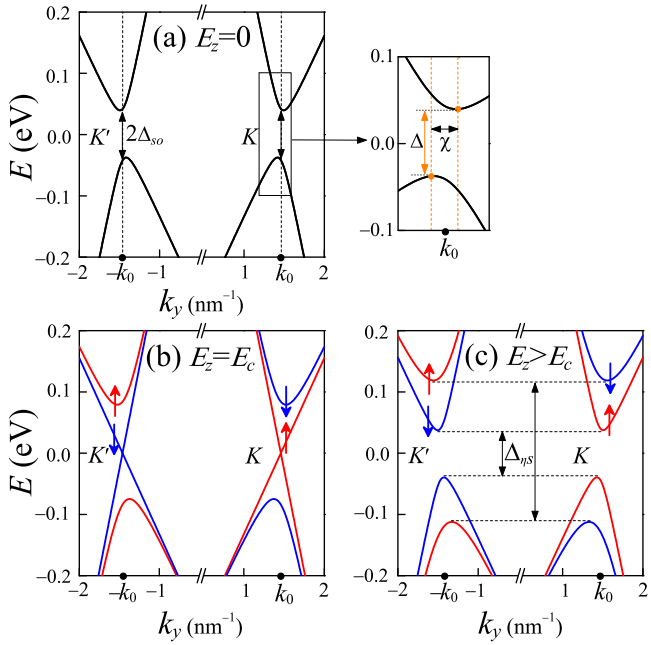

FIG. 1. Band structures around the two Dirac points for monolayer $1T'$-MoS_2 under a vertical electric field of (a) $E_z = 0$, (b) $E_z = E_c$, and (c) $E_z > E_c$. For $E_z = 0$, the spin-orbit coupling gaps $2\Delta_{so}$ at the Dirac points are shown in (a), and the indirect nature of the gap near the K valley is illustrated in the inset of (a), in which the two pink dots correspond to the minimum and maximum of the band branches. Here, Δ is the magnitude of the indirect band gap, and χ denotes the corresponding wave vector shift. In (b) and (c), the red and blue lines represent the spin splitting of the doubly degenerate bands around the Dirac points due to the vertical electric field, and then the indirect band gaps $\Delta_{\eta s}$ become valley and spin dependent.

negative-energy region ($E_{\eta s}^{-,\mathrm{t}}$) as functions of the reduced electric field $\widetilde{E}_z$, where reduced $\widetilde{E}_z = E_z/E_c$ is a unitless variable. One can see that for $\eta s = -1$ subbands, the energy difference $\Delta E_{\eta s=-1}$ between $E_{\eta s}^{+,\mathrm{b}}$ and $E_{\eta s}^{-,\mathrm{t}}$ increases with increasing $\widetilde{E}_z$, while for $\eta s = 1$ subbands, the energy difference $\Delta E_{\eta s=1}$ first decreases to zero at $\widetilde{E}_z = 1$ and then increases gradually with $\widetilde{E}_z$. This is due to $\Delta E_{\eta s=-1} \propto (1 + \widetilde{E}_z)\Delta_{\mathrm{so}}$, but $\Delta E_{\eta s=1} \propto |1 - \widetilde{E}_z|\Delta_{\mathrm{so}}$, as referred to Eq. (12). In addition, it can also be seen that when $\varepsilon_{\mathrm{F}} > \Delta_{\mathrm{so}}$, for $0 < \widetilde{E}_z < \widetilde{E}_{z1}$, all the values of $E_{\eta s}^{+,\mathrm{b}}$ are smaller than ε_{F}, and then the Fermi level intersects with each subband; for $\widetilde{E}_{z1} < \widetilde{E}_z < \widetilde{E}_{z2}$, only $E_{\eta s=1}^{+,\mathrm{b}}$ is smaller than ε_{F}, and then the Fermi level only crosses the $K\uparrow$ and $K'\downarrow$ subbands; for $\widetilde{E}_z > \widetilde{E}_{z2}$, all values of $E_{\eta s}^{+,\mathrm{b}}$ are larger than ε_{F}, and then the Fermi level drops into the band gap. Here, $\widetilde{E}_{z1}$ and $\widetilde{E}_{z2}$ can be determined by Eq. (8), which read

$$\widetilde{E}_{z1} = \frac{(v_2^2 + v_+^2)\varepsilon_{\mathrm{F}}}{\left(v_+\sqrt{v_2^2 + v_+^2 - v_-^2} + v_2 v_-\right)\Delta_{\mathrm{so}}} - 1,$$
$$\widetilde{E}_{z2} = \frac{(v_2^2 + v_+^2)\varepsilon_{\mathrm{F}}}{\left(v_+\sqrt{v_2^2 + v_+^2 - v_-^2} - v_2 v_-\right)\Delta_{\mathrm{so}}} + 1. \quad (13)$$

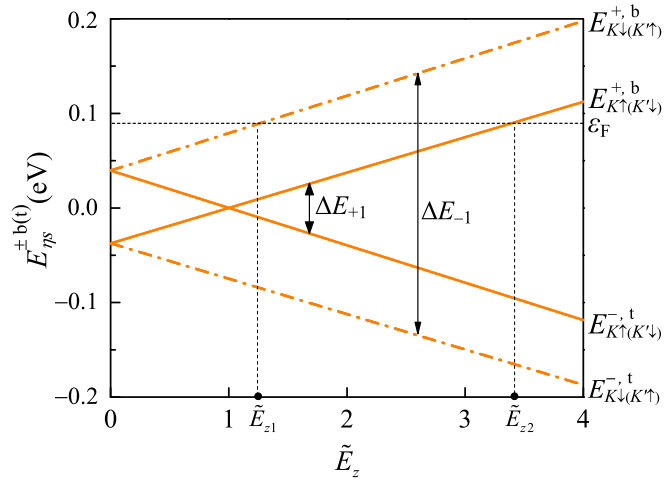

FIG. 2. Minimum and maximum of valley-spin resolved bands near the Dirac points as functions of the reduced electric field $\widetilde{E}_z$ ($\widetilde{E}_z = E_z/E_c$). Here, $\Delta E_{\eta s}$ is the energy difference between the corresponding band branches. The horizontal dashed line indicates the Fermi level ε_{F} lying in the positive-energy region. $\widetilde{E}_{z1}$ and $\widetilde{E}_{z2}$ are the specific electric-field values when the Fermi level intersects with the valley-spin resolved subbands, respectively.

III. TRANSMISSION PROBABILITY OF TILTED *n-p-n* JUNCTION

Next, we consider a tilted *n-p-n* junction of monolayer $1T'$-MoS_2, in which the junction is rotated by an angle θ in the xy plane with respect to the x axis, as schematically shown in Fig. 3. Here and thereafter, the normal (tangential) direction of the junction interface is defined as the x' (y') axis of the coordinate system x'-y'. Then, the Hamiltonian of the tilted junction is given by

$$\mathcal{H}_\eta = \mathcal{H}'_\eta + V_0\Theta(x')\Theta(L - x'), \quad (14)$$

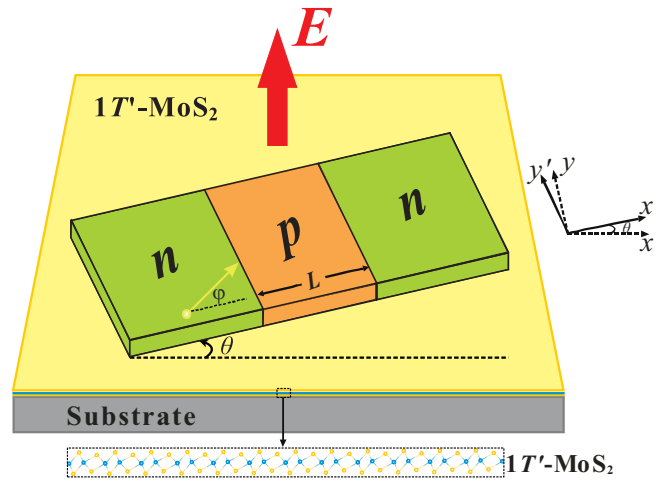

FIG. 3. Schematic diagram of a tilted *n-p-n* junction of monolayer $1T'$-MoS_2 under a vertical electric field. Here, the direction of the tilted junction is characterized by angle θ, while the incident electron is in the direction deviated from the x' axis with angle φ.

where Θ is the Heaviside step function, and L denotes the length of the potential barrier. The electric potential V_0 can be adjusted by a gate voltage or doping. The transformation relationship between the wave vector components in the coordinate systems x-y and x'-y' can be expressed as

$$\begin{aligned} k_x &= k_{x'}\cos\theta - k_{y'}\sin\theta, \\ k_y &= k_{x'}\sin\theta + k_{y'}\cos\theta. \end{aligned} \tag{15}$$

In the coordinate system x'-y', the diagonal blocks in Eq. (4) can be rewritten as

$$\begin{aligned} \boldsymbol{h}_{\eta s}(\boldsymbol{k}) &= \hbar S_x k_{x'} + \hbar S_y k_{y'} + \hbar k_0(v_-\tau_0 + v_+\tau_z + \eta s v_2\tau_x) \\ &\quad + (\widetilde{E}_z - \eta s)\Delta_{\rm so}\tau_x, \end{aligned} \tag{16}$$

where

$$\begin{aligned} S_x &= v_1\tau_y\cos\theta - (\eta v_-\tau_0 + \eta v_+\tau_z + s v_2\tau_x)\sin\theta, \\ S_y &= -v_1\tau_y\sin\theta - (\eta v_-\tau_0 + \eta v_+\tau_z + s v_2\tau_x)\cos\theta. \end{aligned} \tag{17}$$

Correspondingly, in the coordinate system x'-y', the wave functions in the left, middle, and right regions of such a tilted n-p-n junction can be expressed as

$$\begin{aligned} \psi_{\rm L} &= \psi^i_{{\rm L},\eta\uparrow(\downarrow)} + r\psi^r_{{\rm L},\eta\uparrow(\downarrow)}, \\ \psi_{\rm M} &= a\psi^i_{{\rm M},\eta\uparrow(\downarrow)} + b\psi^r_{{\rm M},\eta\uparrow(\downarrow)}, \\ \psi_{\rm R} &= t\psi^t_{{\rm R},\eta\uparrow(\downarrow)}. \end{aligned} \tag{18}$$

The wave functions in each region can be determined by solving the eigenequation of the Hamiltonian in Eq. (14) [47]. So, the transmission coefficient t through this tilted junction can then be straightforwardly obtained by matching the wave functions at $x' = 0$ and $x' = L$.

By means of the continuity equation for the probability density [48,49]

$$\frac{\partial\rho}{\partial t} + \nabla\cdot\mathbf{j} = 0, \tag{19}$$

with $\rho = \phi^\dagger\phi$, we can get the probability current in the tilted n-p-n junction, i.e.,

$$\mathbf{j} = (j_{x'}, j_{y'}) = (\phi^\dagger S_x\phi, \phi^\dagger S_y\phi), \tag{20}$$

where ϕ is the corresponding eigenvector of $\boldsymbol{h}_{\eta s}(\boldsymbol{k})$ in Eq. (16). In our system, the probability current along the x' direction is conserved, and then the transmission probability reads

$$T = \frac{j_{x't}}{j_{x'i}}, \tag{21}$$

in which the incident probability current $j_{x'i} = (\phi^i)^\dagger S_x\phi^i$ and the transmitted probability current $j_{x't} = t^*t(\phi^t)^\dagger S_x\phi^t$. Since the incident and transmitted wave functions are the same in the n-p-n junction considered here, i.e., $\phi^i = \phi^t$, thus the transmission probability is reduced to $T = t^*t$.

IV. VALLEY- AND SPIN-DEPENDENT ELECTRON RETROREFLECTION

First, using Eqs. (8) and (15), we get the velocity components of an electron in the junction,

$$\begin{aligned} u^{\eta s}_{x'} &= \frac{\partial E^+_{\eta s}}{\hbar\partial k_{x'}} = -\eta v_-\sin\theta + \frac{\hbar v_1^2 k_x\cos\theta + \hbar\left(v_+^2 + v_2^2\right)k'_y\sin\theta + (\eta - s\widetilde{E}_z)v_2\Delta_{\rm so}\sin\theta}{\sqrt{(\hbar v_1 k_x)^2 + (\hbar v_+ k'_y)^2 + [\hbar v_2 k'_y + (\eta - s\widetilde{E}_z)\Delta_{\rm so}]^2}}, \\ u^{\eta s}_{y'} &= \frac{\partial E^+_{\eta s}}{\hbar\partial k_{y'}} = -\eta v_-\cos\theta - \frac{\hbar v_1^2 k_x\sin\theta - \hbar\left(v_+^2 + v_2^2\right)k'_y\cos\theta - (\eta - s\widetilde{E}_z)v_2\Delta_{\rm so}\cos\theta}{\sqrt{(\hbar v_1 k_x)^2 + (\hbar v_+ k'_y)^2 + [\hbar v_2 k'_y + (\eta - s\widetilde{E}_z)\Delta_{\rm so}]^2}}, \end{aligned} \tag{22}$$

which depend on valley and spin indices. In Fig. 4, we show the valley- and spin-dependent transverse velocity $u^{\eta s}_{y'i}$ ($u^{\eta s}_{y'r}$) of the incident (reflected) electron in the tilted junction with $\theta = \pi/6$ as functions of the transverse wave vector $k_{y'}$ for the three different electric fields. It can be seen that there are always the $k_{y'}$ intervals that satisfy the electron retroreflection condition as $u^{\eta s}_{y'i}\cdot u^{\eta s}_{y'r} < 0$ in the tilted junction, regardless of the presence or absence of the electric field. The intervals can be determined by the values of $k_{y'}$ at $u^{\eta s}_{y'i} = 0$ and $u^{\eta s}_{y'r} = 0$, as marked by the solid and open circles in Figs. 4(a)– 4(c). It is easy to find from Eq. (22) that for the case of $\theta \neq 0$, $u^{\eta s}_{y'i}$ and $u^{\eta s}_{y'r}$ are no longer identical, and there is the possibility for $u^{\eta s}_{y'i}\cdot u^{\eta s}_{y'r} < 0$, which leads to the release of the locking relation between the transverse wave vector and the corresponding velocity component in the tilted junction and makes electron retroreflection appear. Moreover, it can also be seen that under an electric field, the $k_{y'}$ intervals for electron retroreflection to occur are valley and spin dependent, as shown in Figs. 4(b) and 4(c). In particular, for $\widetilde{E}_{z1} < \widetilde{E}_z < \widetilde{E}_{z2}$, the retroreflection of only electrons with $\eta s = 1$ may occur. This is mainly because in this case the Fermi level intersects only with the $K\uparrow$ and $K'\downarrow$ subbands of monolayer $1T'$-MoS_2.

To explore the electron retroreflection in a tilted junction with different tilt angles θ, in Figs. 4(d)– 4(f) we display the contour lines of $u^{\eta s}_{y'i} = 0$ and $u^{\eta s}_{y'r} = 0$ as functions of θ and $k_{y'}$. One can see that for $0 < \theta < \pi/2$, electron retroreflection always occurs and is valley and spin dependent under the electric field $\widetilde{E}_z$, as shown in Figs. 4(e) and 4(f). Especially, for $\theta = 0$, electron retroreflection cannot happen in the junction. It is due to the fact that for $\theta = 0$, as known from Eq. (22), $u^{\eta s}_{y'i}$ and $u^{\eta s}_{y'r}$ are always equal, which does not satisfy the retroreflection condition of $u^{\eta s}_{y'i}\cdot u^{\eta s}_{y'r} < 0$. On the other hand, it can be obtained from Eq. (22) that for $\theta = \pi/2$, the transverse velocity of incident (reflected) electron is then reduced to

$$u^{\eta s}_{y'i(r)} = \frac{\hbar k_{y'} v_1^2}{\varepsilon + \hbar\eta v_-\left(k^{\eta s}_{x'i(r)} - \eta k_0\right)}, \tag{23}$$

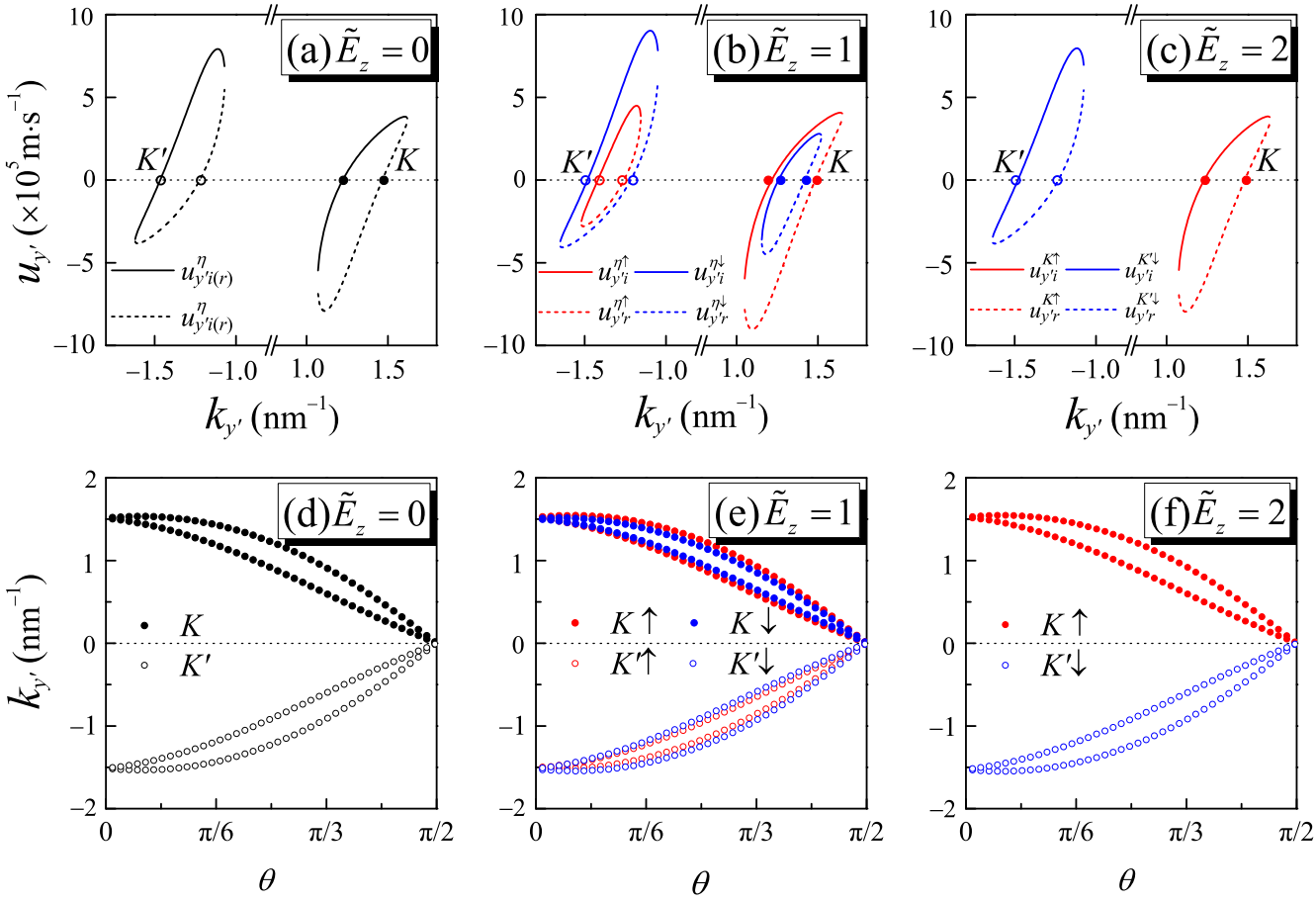

FIG. 4. (a)–(c) Dependence of the group velocity component parallel to the interface ($u_{y'}$) on the transverse wave vector $k_{y'}$ for the three different electric field strengths: (a) $\widetilde{E}_z = 0$, (b) $\widetilde{E}_z = 1$, and (c) $\widetilde{E}_z = 2$ within the range $\widetilde{E}_{z1} < \widetilde{E}_z < \widetilde{E}_{z2}$. Here, $\varepsilon = 0.1$ eV and $\theta = \pi/6$. $u^{\eta}_{y'i(r)}$ denotes the transverse velocity of incident (reflected) electron from each valley. The solid and open circles are used to mark the values of $k_{y'}$ at $u^{\eta s}_{y'i(r)} = 0$. (d)–(f) Contour lines of $u^{\eta s}_{y'i(r)} = 0$ as functions of the transverse wave vector $k_{y'}$ and tilt angle of the junction θ for the above values of $\widetilde{E}_z$.

which indicates that in this case the $k_{y'}$ intervals for electron retroreflection to occur disappear at $k_{y'} = 0$.

Considering that it is inconvenient to adjust the tilt angle of the junction for a given device in practical operations, in Fig. 5 we further illustrate the contour lines of $u^{\eta s}_{y'i} = 0$ and $u^{\eta s}_{y'r} = 0$ as functions of the electric field $\widetilde{E}_z$ and $k_{y'}$ at a given θ. It is clearly seen that the $k_{y'}$ intervals for electron retroreflection to occur depend on the electric field $\widetilde{E}_z$. For $\widetilde{E}_z < \widetilde{E}_{z1}$, since the Fermi level crosses each subband in the conduction band, as can be seen also in Fig. 2, then spin-up and spin-down electrons from each valley can be retroreflected in the tilted junction. While for $\widetilde{E}_{z1} < \widetilde{E}_z < \widetilde{E}_{z2}$, the Fermi level only intersects with the $\eta s = 1$ subbands, then the retroreflection of $K\uparrow$ and $K'\downarrow$ electrons may occur. Therefore, the vertical electric field can effectively modulate the valley- and spin-dependent electron retroreflection in the tilted junction.

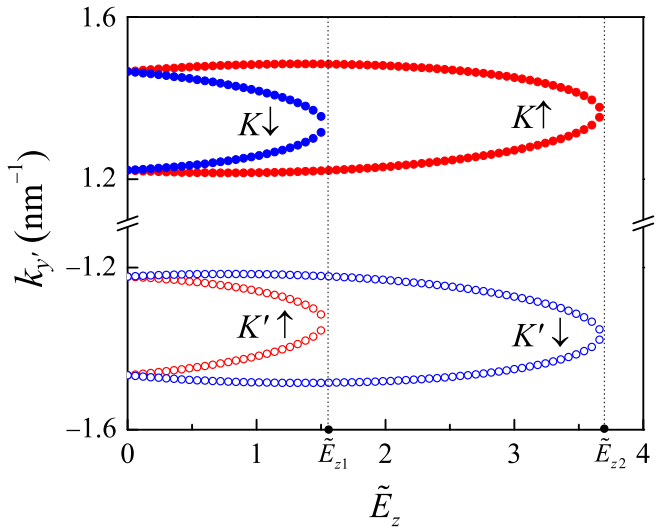

FIG. 5. Contour lines of $u^{\eta s}_{y'i(r)} = 0$ as functions of the transverse wave vector $k_{y'}$ and the electric field $\widetilde{E}_z$ at $\theta = \pi/6$. The other parameter values are as in Fig. 4.

V. VALLEY- AND SPIN-DEPENDENT KLEIN TUNNELING

Using the Heisenberg equation of motion, we can obtain the velocity operator along the x' direction, i.e., $\hat{u}_{x'} =$

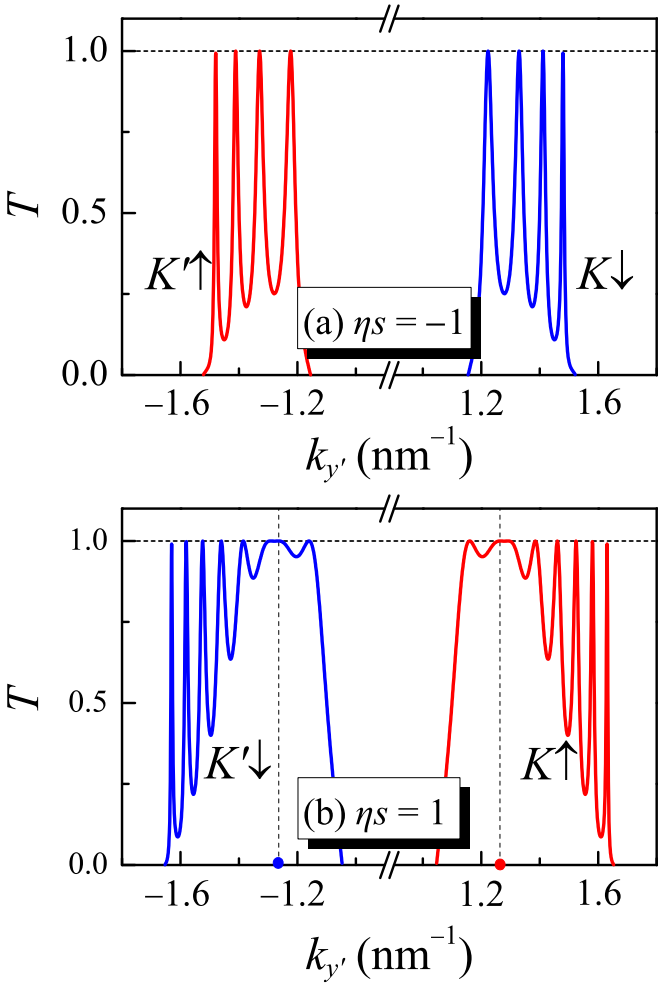

FIG. 6. Dependence of electronic transmission probability in the tilted *n*-*p*-*n* junction with $\theta = \pi/6$ on the transverse wave vector $k_{y'}$ under an electric field of $\widetilde{E}_z = 1$. Here, $\varepsilon = 0.1$ eV, $V_0 = 0.5$ eV, and $L = 80$ nm.

$[x', \boldsymbol{h}_{\eta s}]/(i\hbar) = S_x$. Its time evolution is given by

$$\begin{aligned}\dot{\hat{u}}_{x'} &= \frac{1}{i\hbar}[\hat{u}_{x'}, \boldsymbol{h}_{\eta s}] \\ &= 2v_1(k_{y'} - \eta k_0 \cos\theta)(sv_2\tau_z - \eta v_+\tau_x) \\ &\quad - \frac{2\Delta_{\rm so}}{\hbar}(\widetilde{E}_z - \eta s)(v_1 \cos\theta\tau_z + \eta v_+ \sin\theta\tau_y). \quad (24)\end{aligned}$$

Due to the translational invariance along the y' direction, the transverse wave vector $k_{y'}$ is conserved. The result in Eq. (24) reveals that when $k_{y'} = \eta k_0 \cos\theta$, the velocity along the x' axis of the $K\uparrow$ or $K'\downarrow$ electron is conserved in the case of $\widetilde{E}_z = 1$, which means the appearance of Klein tunneling with $T \equiv 1$. To verify the above analysis, we calculate the valley- and spin-dependent transmission probability T of an electron in the tilted junction with $\theta = \pi/6$ versus the transverse wave vector $k_{y'}$ at $\widetilde{E}_z = 1$, as shown in Fig. 6. It is seen that since the energy gaps of the $K\uparrow$ and $K'\downarrow$ subbands decrease to zero at $\widetilde{E}_z = 1$, then only an electron with $\eta s = 1$ can undergo the Klein tunneling in the case of $k_{y'} = \eta k_0 \cos\pi/6 \approx \pm 1.26$ nm^{-1}, as indicated by the two vertical dashed lines in Fig. 6(b).

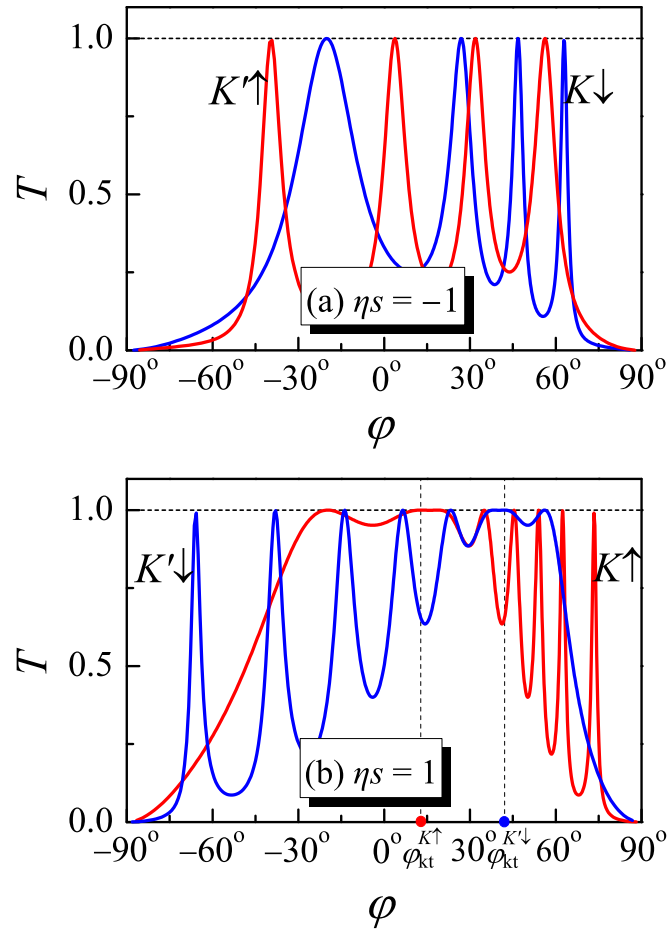

FIG. 7. Electronic transmission probability in the tilted *n*-*p*-*n* junction with $\theta = \pi/6$ vs the incident angle φ under an electric field of $\widetilde{E}_z = 1$. The other parameter values are as in Fig. 6.

In order to further demonstrate the Klein tunneling of a massless Dirac electron in the tilted *n*-*p*-*n* junction of monolayer $1T'$-MoS_2, in Fig. 7 we plot the valley- and spin-dependent transmission probability of an electron in the tilted junction with $\theta = \pi/6$ as a function of the incident angle φ under an electric field of $\widetilde{E}_z = 1$. Here, the incident angle of an electron is defined as

$$\varphi = \arctan\frac{u_{y'i}^{\eta s}}{u_{x'i}^{\eta s}}. \quad (25)$$

According to Eqs. (24) and (25), we find that in the case of $\widetilde{E}_z = 1$, only an electron with $\eta s = 1$ can undergo the Klein tunneling at $\varphi_{\rm kt}^{K\uparrow} \approx 12.8^\circ$ and $\varphi_{\rm kt}^{K'\downarrow} \approx 42.1^\circ$, as marked by the red and blue dots in Fig. 7(b). Besides these incident angles for the Klein tunneling, in Fig. 7 there are other incident angles with $T = 1$, corresponding to the resonant tunneling of electrons. Unlike the incident angles for the Klein tunneling, these angles for resonant tunneling are very sensitive to the width and height of a potential barrier and the incident electron energy.

Since perfect transmission ($T \equiv 1$) in the tilted junction should satisfy the condition of $k_{y'} = \eta k_0 \cos\theta$ at $\widetilde{E}_z = 1$, thus the incident angles of Klein tunneling in the system depend on the direction of the junction, as can be seen in Fig. 8. Under

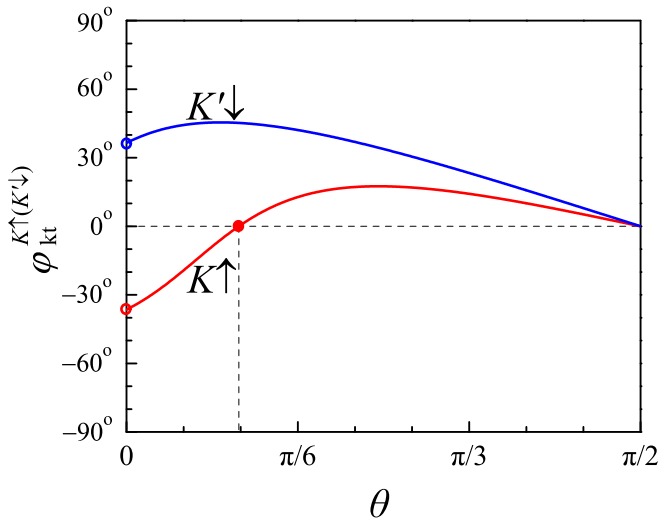

FIG. 8. Valley- and spin-dependent incident angle of Klein tunneling $\varphi_{kt}^{K\uparrow(K'\downarrow)}$ vs the tilt angle of the junction θ under an electric field of $\widetilde{E}_z = 1$.

an electric field of $\widetilde{E}_z = 1$, for $\theta = 0$, the incident angles of Klein tunneling $\varphi_{kt}^{K\uparrow(K'\downarrow)} = \arctan(-\eta v_-/v_1) \approx -\eta 36.5^\circ$ by calculating Eq. (25), while for $\theta = \pi/2$, then $\varphi_{kt}^{K\uparrow(K'\downarrow)} = 0$. Generally, for $0 < \theta < \pi/2$, the incident angle of Klein tunneling in the titled *n-p-n* junction can be expressed as

$$\varphi_{kt}^{K\uparrow(K'\downarrow)} = \arctan \frac{\tilde{v}^2 \sin\theta\cos\theta - \eta v_- \cos\theta\sqrt{v_1^2 + \tilde{v}^2\sin\theta^2}}{v_1^2 + \tilde{v}^2\sin\theta^2 - \eta v_- \sin\theta\sqrt{v_1^2 + \tilde{v}^2\sin\theta^2}}, \tag{26}$$

with $\tilde{v} = \sqrt{v_2^2 + v_+^2 - v_1^2}$. It is found from Eq. (26) that when $\theta = \arcsin(v_1 v_-/\tilde{v}\sqrt{\tilde{v}^2 - v_-^2}) \approx \pi/9$, then $\varphi_{kt}^{K\uparrow} = 0$, as marked by the red solid circle in Fig. 8. This result indicates that in the case of normal incidence, the phenomenon of Klein tunneling happens only for the $K\uparrow$ electron in the titled *n-p-n* junction.

VI. CONCLUSIONS

In summary, we have investigated the electronic transport properties in a tilted *n-p-n* junction of monolayer $1T'$-MoS_2 subjected to a vertical electric field. It was shown that valley- and spin-dependent electron retroreflection can be generated in this tilted junction, which arises from the anisotropic band structure of monolayer $1T'$-MoS_2, and the exotic electron retroreflection can be modulated by the electric field. We also found that when the electric field is adjusted to a critical value (∼0.142 V/Å), the phenomenon of valley- and spin-dependent Klein tunneling occurs in the junction, and the incident angle of the Klein tunneling is strongly dependent on the tilt angle of the junction. Especially, for a specific tilt angle ($\sim\pi/9$), in the case of normal incidence, only a spin-up electron from the K valley can undergo Klein tunneling. It is expected that the above results are qualitatively valid for other monolayer TMDCs with a $1T'$ structure due to the similarity of their band structures. Our work offers an efficient mechanism to modulate valley- and spin-dependent electron retroreflection and Klein tunneling in anisotropic tilted Dirac systems.

ACKNOWLEDGMENTS

This work was supported by the National Natural Science Foundation of China (Grants No. 11047019 and No. 12074156) and the Anhui Provincial Natural Science Foundation (Grant No. 1408085MA15).

[1] C.-C. Liu, H. Jiang, and Y. Yao, Phys. Rev. B **84**, 195430 (2011).
[2] M. E. Dávila, L. Xian, S. Cahangirov, A. Rubio, and G. Le Lay, New J. Phys. **16**, 095002 (2014).
[3] F.-f. Zhu, W.-j. Chen, Y. Xu, C.-l. Gao, D.-d. Guan, C.-h. Liu, D. Qian, S.-C. Zhang, and J.-f. Jia, Nat. Mater. **14**, 1020 (2015).
[4] L. Li, Y. Yu, G. J. Ye, Q. Ge, X. Ou, H. Wu, D. Feng, X. H. Chen, and Y. Zhang, Nat. Nanotechnol. **9**, 372 (2014).
[5] H. Liu, A. T. Neal, Z. Zhu, Z. Luo, X. Xu, D. Tomanek, and P. D. Ye, ACS Nano **8**, 4033 (2014).
[6] A. Carvalho, M. Wang, X. Zhu, A. S. Rodin, H. Su, and A. H. Castro Neto, Nat. Rev. Mater. **1**, 16061 (2016).
[7] C. Kamal and M. Ezawa, Phys. Rev. B **91**, 085423 (2015).
[8] S. Zhang, Z. Yan, Y. Li, Z. Chen, and H. Zeng, Angew. Chem. Int. Ed. **54**, 3112 (2015).
[9] J. Ji, X. Song, J. Liu, Z. Yan, C. Huo, S. Zhang, M. Su, L. Liao, W. Wang, Z. Ni, Y. Hao, and H. Zeng, Nat. Commun. **7**, 13352 (2016).
[10] A. J. Mannix, X.-F. Zhou, B. Kiraly, J. D. Wood, D. Alducin, B. D. Myers, X. Liu, B. L. Fisher, U. Santiago, J. R. Guest, M. J. Yacaman, A. Ponce, A. R. Oganov, M. C. Hersam, and N. P. Guisinger, Science **350**, 1513 (2015).
[11] B. Feng, J. Zhang, Q. Zhong, W. Li, S. Li, H. Li, P. Cheng, S. Meng, L. Chen, and K. Wu, Nat. Chem. **8**, 563 (2016).
[12] W. Li, L. Kong, C. Chen, J. Gou, S. Sheng, W. Zhang, H. Li, L. Chen, P. Cheng, and K. Wu, Sci. Bull. **63**, 282 (2018).
[13] D. Xiao, G. B. Liu, W. Feng, X. Xu, and W. Yao, Phys. Rev. Lett. **108**, 196802 (2012).
[14] Q. H. Wang, K. Kalantar-Zadeh, A. Kis, J. N. Coleman, and M. S. Strano, Nat. Nanotechnol. **7**, 699 (2012).
[15] X. Qian, J. Liu, L. Fu, and J. Li, Science **346**, 1344 (2014).
[16] X. Xu, W. Yao, D. Xiao, and T. F. Heinz, Nat. Phys. **10**, 343 (2014).
[17] S. Manzeli, D. Ovchinnikov, D. Pasquier, O. V. Yazyev, and A. Kis, Nat. Rev. Mater. **2**, 17033 (2017).
[18] Z. Fei, T. Palomaki, S. Wu, W. Zhao, X. Cai, B. Sun, P. Nguyen, J. Finney, X. Xu, and D. H. Cobden, Nat. Phys. **13**, 677 (2017).
[19] S. Wu, V. Fatemi, Q. D. Gibson, K. Watanabe, T. Taniguchi, R. J. Cava, and P. Jarillo-Herrero, Science **359**, 76 (2018).

[20] V. Fatemi, S. Wu, Y. Cao, L. Bretheau, Q. D. Gibson, K. Watanabe, T. Taniguchi, R. J. Cava, and P. Jarillo-Herrero, Science **362**, 926 (2018).
[21] E. Sajadi, T. Palomaki, Z. Fei, W. Zhao, P. Bement, C. Olsen, S. Luescher, X. Xu, J. A. Folk, and D. H. Cobden, Science **362**, 922 (2018).
[22] Y. Ominato, J. Fujimoto, and M. Matsuo, Phys. Rev. Lett. **124**, 166803 (2020).
[23] F. Zheng, C. Cai, S. Ge, X. Zhang, X. Liu, H. Lu, Y. Zhang, J. Qiu, T. Taniguchi, K. Watanabe, S. Jia, J. Qi, J.-H. Chen, D. Sun, and J. Feng, Adv. Mater. **28**, 4845 (2016).
[24] S. Tang, C. Zhang, D. Wong, Z. Pedramrazi, H.-Z. Tsai, C. Jia, B. Moritz, M. Claassen, H. Ryu, S. Kahn, J. Jiang, H. Yan, M. Hashimoto, D. Lu, R. G. Moore, C.-C. Hwang, C. Hwang, Z. Hussain, Y. Chen, M. M. Ugeda *et al.*, Nat. Phys. **13**, 683 (2017).
[25] Z.-Y. Jia, Y.-H. Song, X.-B. Li, K. Ran, P. Lu, H.-J. Zheng, X.-Y. Zhu, Z.-Q. Shi, J. Sun, J. Wen, D. Xing, and S.-C. Li, Phys. Rev. B **96**, 041108(R) (2017).
[26] L. Peng, Y. Yuan, G. Li, X. Yang, J.-J. Xian, C.-J. Yi, Y.-G. Shi, and Y.-S. Fu, Nat. Commun. **8**, 659 (2017).
[27] B. Das, D. Sen, and S. Mahapatra, Sci. Rep. **10**, 6670 (2020).
[28] C.-Y. Tan, C.-X. Yan, Y.-H. Zhao, H. Guo, and H.-R. Chang, Phys. Rev. B **103**, 125425 (2021).
[29] A. Lopez-Bezanilla and P. B. Littlewood, Phys. Rev. B **93**, 241405(R) (2016).
[30] Y. Ma, L. Kou, X. Li, Y. Dai, and T. Heine, NPG Asia Mater. **8**, e264 (2016).
[31] S. Li, Y. Liu, Z.-M. Yu, Y. Jiao, S. Guan, X.-L. Sheng, Y. Yao, and S. A. Yang, Phys. Rev. B **100**, 205102 (2019).
[32] P.-J. Guo, X.-Q. Lu, W. Ji, K. Liu, and Z.-Y. Lu, Phys. Rev. B **102**, 041109(R) (2020).
[33] K. Sadhukhan and A. Agarwal, Phys. Rev. B **96**, 035410 (2017).
[34] Z. Jalali-Mola and S. A. Jafari, Phys. Rev. B **98**, 195415 (2018).
[35] S. Verma, A. Mawrie, and T. K. Ghosh, Phys. Rev. B **96**, 155418 (2017).
[36] M. A. Mojarro, R. Carrillo-Bastos, and J. A. Maytorena, Phys. Rev. B **103**, 165415 (2021).
[37] SK Firoz Islam and A. M. Jayannavar, Phys. Rev. B **96**, 235405 (2017).
[38] V. H. Nguyen and J.-C. Charlier, Phys. Rev. B **97**, 235113 (2018).
[39] G. C. Paul, SK Firoz Islam, and A. Saha, Phys. Rev. B **99**, 155418 (2019).
[40] P. Kapri, B. Dey, and T. K. Ghosh, Phys. Rev. B **102**, 045417 (2020).
[41] C. W. J. Beenakker, Phys. Rev. Lett. **97**, 067007 (2006).
[42] T. Ludwig, Phys. Rev. B **75**, 195322 (2007).
[43] Y. S. Ang, Z. Ma, and C. Zhang, Sci. Rep. **2**, 1013 (2012).
[44] S.-H. Zhang and W. Yang, Phys. Rev. B **97**, 235440 (2018).
[45] X. Zhou, Phys. Rev. B **100**, 195139 (2019).
[46] S.-H. Zhang and W. Yang, New J. Phys. **21**, 103052 (2019).
[47] See Supplemental Material at http://link.aps.org/supplemental/10.1103/PhysRevB.107.035301 for the derivations of the unitary transformation, the wave functions in each region, and the transmission coefficient.
[48] P. E. Allain and J. N. Fuchs, Eur. Phys. J. B **83**, 301 (2011).
[49] D. Wang, Z. Huang, Y. Zhang, and G. Jin, Phys. Rev. B **93**, 195425 (2016).